

NUMERICAL STUDY ON THE LOCAL WIND STRUCTURES FORCED BY THE COMPLEX TERRAIN OF QINGDAO AREA

Wu Zengmao (吴增茂)

Institute of Physical Oceanography, Ocean University of Qingdao, Qingdao 266003

and K. Heinke Schlunzen

Meteorological Institute, University of Hamburg, 2000 Hamburg 13, F. R. G.

Received March 13, 1991

ABSTRACT

In this paper, some 2-D features of the down- and up-slope winds and sea-land-breeze generated over the complex terrain of the Qingdao area and the interaction between them are numerically analysed by use of a 2-D non-hydrostatic mesoscale model. The simulated results in the west-east vertical cross-section show that (1) when the large-scale wind is a southerly gentle one, the generated easterly down-slope wind is much stronger than with an opposite background wind, and the down-slope wind can trigger and intensify the land breeze corresponding to the eastern coast of Jiaozhou Bay; (2) a gentle westerly background wind will reduce the eastward sea breeze and up-slope wind during the daytime due to a cold advection, but shows a little effect on the mesoscale circulation formed in the nighttime.

Key words: numerical study, local wind structure, complex terrain, Qingdao area

1. INTRODUCTION

Qingdao is a very important harbour and industrial city, and a popular summer resort with a population of about one million. The fast development of industries in recent years has required scientific worker to study the environmental impact of the industrial areas.

The city of Qingdao is situated on a peninsula connecting with Jiaozhou Bay at the west and surrounded by the Huanghai Sea at the south and east sides. The terrain of Qingdao area is very complex. The Laoshan mountains with main peak more than 1100 m are situated east of Qingdao; Fushan and Wushan hills whose peaks are more than 300 m are lying along the southern coastline of the peninsula. Besides, a number of hills lower than 200 m are scattered in Qingdao's urban districts. The mean latitude and longitude of the studied area are $\varphi = 36.1^\circ\text{N}$ and $\lambda = 120.4^\circ\text{E}$.

The atmospheric pollutant transport in the Qingdao area is strongly influenced by the sea-land-breeze and slope-valley wind features developing in the area. Owing to the interactions between sea-land-breeze and slope-valley winds, and both branches of the sea-breezes as well as the effects of the city heat island, Qingdao's local wind presents very complicated temporal and spacial variations. The object of this paper is to study the circulation features of the local wind based on the numerical simulation results.

From comparisons of model simulations with observations it has been concluded that turbulent kinetic energy (TKE) closure models show better agreement with measurements than the first order closure models. Among TKE schemes, as a group, $E-\varepsilon$ parameterizations

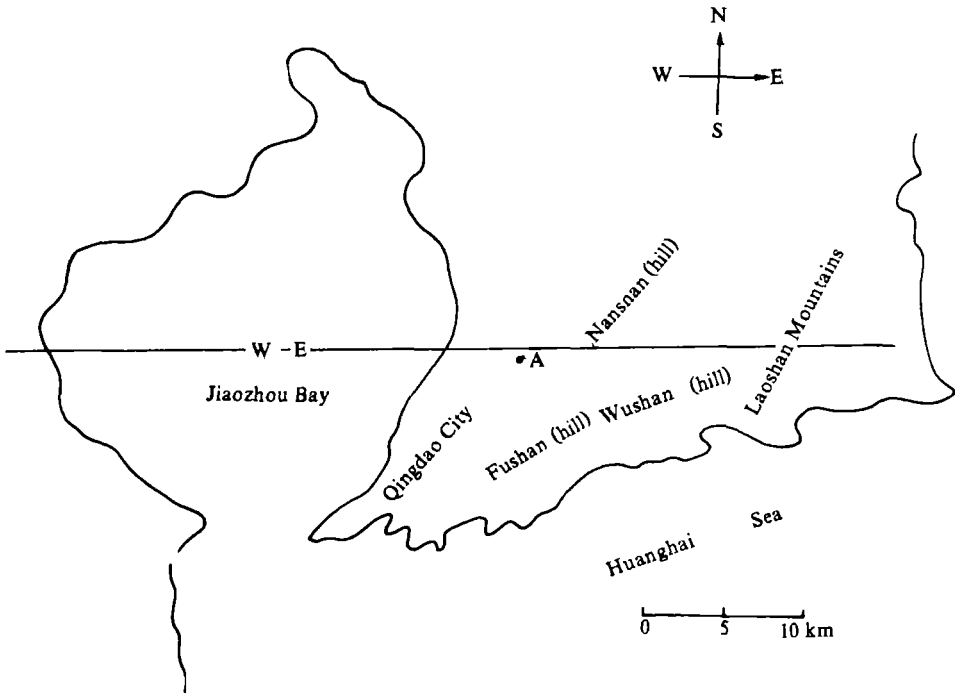


Fig. 1. Schematic map of Qingdao area. The simulated cross-section is marked with W-E.

perform better than E- ϵ schemes (Holt and Ramam, 1988), due to the physically more realistic determination of TKE and dissipation ϵ . This is particularly true in the cases in which the mixing length l is no longer determined by the local surface characteristics, e.g. internal production processes of TKE or the flow over irregular terrain (Duykerke, 1988). In those cases an E- ϵ closure model is able to simulate the atmospheric boundary layer circulation more accurately than an E- l closure model.

In order to study the local wind structure, the mesoscale non-hydrostatic atmospheric model METRAS (Schlunzen, 1988; 1990) is employed. An E- ϵ turbulent closure scheme has been added recently by Wu and Schlunzen. A finer grid is used in the primarily interesting areas of the study.

Although METRAS is a 3-dimensional model and 3-D studies of Qingdao's local wind are necessary, in this paper only 2-D experiments are carried out for limitation of computer resources. The simulated cross-section is selected, as shown in Fig. 1 and marked with W-E, since the eastern coastal area of Jiaozhou Bay, situated in the section, is the Qingdao's old industrial district with dense residents and heavier air pollution, and so its local wind study is interesting and especially emphasised for air pollution control.

II. NUMERICAL MODEL

The main model METRAS is a mesoscale, non-hydrostatic model, where an E- ϵ closure scheme has been added. In this paper only the mesoscale pressure equations and the E- ϵ sub-model are presented. A detailed model description can be found in the works mentioned above.

In the model the dependent variables are decomposed as

$$A = a_0 + \tilde{a} + a' = \bar{a} + a',$$

where A represents anyone of the wind components (u, v, w), temperature (θ) and pressure (p). a_0 is the synoptic scale value, \tilde{a} the mesoscale, and a' the subgrid scale value whose effects will be parameterized. A terrain-following coordinate η is applied, $\eta = z_{\text{top}}[z - z_s(x, y)] / [z_{\text{top}} - z_s(x, y)]$, and a nonuniform horizontal and vertical grid is utilized with the following transformation:

$$\dot{x}^1 = \dot{x}^1(x), \quad \dot{x}^2 = \dot{x}^2(y), \quad \dot{x}^3 = \dot{x}^3(\eta). \tag{1}$$

1. Model Equations

In model METRAS the mesoscale perturbation pressure \tilde{p} is composed of p_1 and p_2 . p_1 corresponds to the hydrostatic pressure portion and is determined diagnostically by

$$\frac{\partial p_1}{\partial \dot{x}^3} = -g \rho_0 \frac{\tilde{\rho}}{\rho_0} \frac{\partial z}{\partial \dot{x}^3}. \tag{2}$$

The mesoscale density perturbation $\tilde{\rho}$ is mainly dependent on temperature perturbation $\tilde{\theta}$ but might be influenced by pressure perturbation \tilde{p} for deep convection. $\tilde{\rho} = \rho_0 [(-\tilde{\theta} / \theta) + (C_v / C_p) \cdot (\tilde{p} / p_0)]$ is used in Eq. (2).

The dynamic pressure portion p_2 is calculated from the elliptic differential equation (3), which is derived from the anelastic equation:

$$\begin{aligned} \nabla^2 p_2 = & \frac{1}{\Delta t} \left\{ \frac{\partial}{\partial \dot{x}^1} \left(\rho_0 \alpha^* \hat{u} \frac{\partial \dot{x}^1}{\partial x} \right) + \frac{\partial}{\partial \dot{x}^2} \left(\rho_0 \alpha^* \hat{v} \frac{\partial \dot{x}^2}{\partial y} \right) \right\} \\ & + \frac{1}{\Delta t} \frac{\partial}{\partial \dot{x}^3} \left(\rho_0 \alpha^* \hat{u} \frac{\partial \dot{x}^3}{\partial x} + \rho_0 \alpha^* \hat{v} \frac{\partial \dot{x}^3}{\partial y} + \rho_0 \alpha^* \hat{w} \frac{\partial \dot{x}^3}{\partial z} \right), \end{aligned} \tag{3}$$

where $\hat{u}, \hat{v}, \hat{w}$ are, respectively, the temporary values of \bar{u}, \bar{v} and \bar{w} which do not include effects of p_2 ; \dot{x}^i and \dot{u}^i ($i = 1, 2, 3$) are the terrain-following coordinates and the corresponding wind components:

$$\begin{aligned} \dot{u}^1 &= \bar{u}(\partial \dot{x}^1 / \partial x), \\ \dot{u}^2 &= \bar{v}(\partial \dot{x}^2 / \partial y), \\ \dot{u}^3 &= \bar{u}(\partial \dot{x}^3 / \partial x) + \bar{v}(\partial \dot{x}^3 / \partial y) + \bar{w}(\partial \dot{x}^3 / \partial z), \end{aligned}$$

α^* is the grid volume. The other symbols in the above equations have their normal meaning in meteorological parlance.

In the general Cartesian coordinate system, the turbulent kinetic energy (TKE) is defined as $E = 0.5(u'^2 + v'^2 + w'^2)$, and the TKE equation is written as

$$\frac{\partial \bar{E}}{\partial t} + \bar{u}_j \frac{\partial \bar{E}}{\partial x_j} = -\overline{u'_i u'_j} \frac{\partial \bar{u}_i}{\partial x_j} + \delta_{i3} \frac{g}{\theta} (\overline{u'_i \theta'}) - \frac{\partial \overline{u'_j E}}{\partial x_j} - \frac{\partial (\overline{u'_j p'} / \rho_0)}{\partial x_j} - \varepsilon. \tag{4}$$

With neglect of small terms, the above equation can be rewritten as

$$\frac{\partial \bar{E}}{\partial t} + \left(\bar{u}_j \frac{\partial \bar{E}}{\partial x_j} \right)_{j=1,2,3}^{(1)} = \left(-\overline{u'_i w'} \frac{\partial \bar{u}_i}{\partial z} \right)_{i=1,2}^{(2)} + \left(\frac{g}{\theta} (\overline{w' \theta'}) \right)^{(3)}$$

$$- \left(\frac{\partial(\overline{w'E})}{\partial z} \right)^{(4)} - \left(\frac{\partial(\overline{w'p'/\rho_0})}{\partial z} \right)^{(5)} - \varepsilon + (\overline{F_H})^{(6)}.$$

Here term (1) (referred as ADV) is the advection of TKE, term (2) (PS) corresponds to the shear production rate of TKE, and term (3) (PB) to the buoyancy production rate, which are both parameterized in the usual way. The viscous dissipation term ε is calculated by use of a prognostic equation. The horizontal diffusion term (6) (HD) will be simply replaced by a horizontal filter (Pepper et al., 1979). The pressure perturbation transfer term (5) (PPT) and the energy gradient transport term (4) (EGT) are also parameterized in the normal way:

$$- \frac{\partial(\overline{w'E})}{\partial z} - \frac{\partial(\overline{w'p'/\rho_0})}{\partial z} = \frac{\partial}{\partial z} \left(K_e \frac{\partial \overline{E}}{\partial z} \right) = \alpha_E \frac{\partial}{\partial z} \left(K_m \frac{\partial \overline{E}}{\partial z} \right).$$

The parameterized form of TKE equation results in

$$\begin{aligned} \frac{\partial \overline{E}}{\partial t} + \overline{u}_j \frac{\partial \overline{E}}{\partial x_j} &= K_m \left[\left(\frac{\partial \overline{u}}{\partial z} \right)^2 + \left(\frac{\partial \overline{v}}{\partial z} \right)^2 \right] - \frac{g}{\theta} K_h \left(\frac{\partial \overline{\theta}}{\partial z} - R_{cg} \right) \\ &+ \alpha_E \frac{\partial}{\partial z} \left(K_m \frac{\partial \overline{E}}{\partial z} \right) - \varepsilon + \overline{F_H}, \end{aligned}$$

where R_{cg} is the counter-gradient heat flux correction (Wu, 1987). K_m , K_e are turbulent transfer coefficients for momentum and TKE respectively. α_E is the ratio of K_e to K_m , in this study $\alpha_E = 1.35$ given by Detering and Etling (1985) is used.

In the terrain-following coordinate system the TKE equation is given by

$$\begin{aligned} \frac{\partial \rho_0 \alpha^* \overline{E}}{\partial t} + \rho_0 \alpha^* \left(\dot{u}^1 \frac{\partial \overline{E}}{\partial \dot{x}^1} + \dot{u}^2 \frac{\partial \overline{E}}{\partial \dot{x}^2} + \dot{u}^3 \frac{\partial \overline{E}}{\partial \dot{x}^3} \right) \\ = \rho_0 \alpha^* K_m \left[\left(\frac{\partial \overline{u}}{\partial \dot{x}^3} \right)^2 + \left(\frac{\partial \overline{v}}{\partial \dot{x}^3} \right)^2 + \left(\frac{\partial \overline{w}}{\partial \dot{x}^3} \right)^2 \right] / \left(\frac{\partial \eta}{\partial \dot{x}^3} \right)^2 \\ - \rho_0 \alpha^* \frac{g}{\theta} K_h \left(\frac{\partial \overline{\theta}}{\partial \dot{x}^3} - R_{cg} \right) / \left(\frac{\partial \eta}{\partial \dot{x}^3} \right) \\ + \alpha_E \frac{\partial}{\partial \dot{x}^3} \left[\rho_0 \alpha^* K_m \left(\frac{\partial \overline{E}}{\partial \dot{x}^3} / \frac{\partial \eta}{\partial \dot{x}^3} \right) \right] / \left(\frac{\partial \eta}{\partial \dot{x}^3} \right) - \rho_0 \alpha^* \varepsilon. \end{aligned} \quad (5)$$

The parameterized form of the equation for dissipation ε in the terrain-following coordinate system is obtained in the same way as the above:

$$\begin{aligned} \frac{\partial \rho_0 \alpha^* \varepsilon}{\partial t} + \rho_0 \alpha^* \left(\dot{u}^1 \frac{\partial \varepsilon}{\partial \dot{x}^1} + \dot{u}^2 \frac{\partial \varepsilon}{\partial \dot{x}^2} + \dot{u}^3 \frac{\partial \varepsilon}{\partial \dot{x}^3} \right) \\ = C_{E1} \frac{\varepsilon}{E} \rho_0 \alpha^* K_m \left[\left(\frac{\partial \overline{u}}{\partial \dot{x}^3} \right)^2 + \left(\frac{\partial \overline{v}}{\partial \dot{x}^3} \right)^2 + \left(\frac{\partial \overline{w}}{\partial \dot{x}^3} \right)^2 \right] / \left(\frac{\partial \eta}{\partial \dot{x}^3} \right)^2 \\ - C_{E1} \frac{\varepsilon}{E} \rho_0 \alpha^* (1 - C_{E2}) \frac{g}{\theta} K_h \left(\frac{\partial \overline{\theta}}{\partial \dot{x}^3} - R_{cg} \right) / \left(\frac{\partial \eta}{\partial \dot{x}^3} \right) \\ - C_{E3} \rho_0 \alpha^* \frac{\varepsilon^2}{E} + \frac{1}{C_{E4}} \frac{\partial}{\partial \dot{x}^3} \left[\rho_0 \alpha^* K_m \left(\frac{\partial \varepsilon}{\partial \dot{x}^3} / \frac{\partial \eta}{\partial \dot{x}^3} \right) \right] / \left(\frac{\partial \eta}{\partial \dot{x}^3} \right). \end{aligned} \quad (6)$$

In this study $\langle C_{E1}, C_{E3}, C_{E4}, C_{E5} \rangle = \langle 1.46, 1.83, 2.39, 0.19 \rangle$ (Duynderke, 1988), and

$$C_{E2} = \begin{cases} 0 & \text{when the buoyancy production rate of TKE is positive,} \\ 1.0 & \text{else.} \end{cases}$$

The exchange coefficient for momentum K_m is calculated as

$$K_m = \frac{(C_{E5} \bar{E})^2}{\varepsilon}, \quad (7)$$

and the exchange coefficient for heat $K_h = 1.35K_m$ is used.

The horizontal diffusion coefficients are calculated according to the vertical diffusion coefficients K_{vert} (K_m, K_h) (Dunst, 1980),

$$K_{\text{hor}} = 0.5 \frac{(\Delta x^2 + \Delta y^2)^{1/2}}{\Delta \eta} K_{\text{vert}}. \quad (8)$$

For 2-D case, $K_{\text{hor}} = 0.5(\Delta x / \Delta \eta) K_{\text{vert}}$.

2. The Boundary and Initial Conditions

A complete description of the boundary conditions of METRAS is presented in Schlunzen (1988). In this paper only 2-D experiment conditions are discussed. For the lateral boundary conditions, the radiation conditions are applied for the normal component of the wind vector (after Orlanski, 1976), and no-gradient conditions are utilized for the remaining wind components and for the scalar values $T, p_2, E,$ and ε .

At the upper boundary of the model, an absorbing layer is implemented for the velocities. A no-gradient assumption is used for TKE and ε equations. At the lower boundary the land surface temperature T_s is derived from the energy budget equation in the way:

$$\frac{\partial T_s}{\partial t} = \frac{2K_s}{\gamma_s h} (\mu I_s \cos Z(t))^{(1)} - \frac{2K_s}{\gamma_s h} \left[\left(\hat{\varepsilon} \sigma T_s^4 \right)^{(2)} - (c_p \rho_0 \theta, u_s)^{(3)} + \left(\gamma_s \frac{T_s - T(-h)}{h} \right)^{(4)} \right], \quad (9)$$

where terms (1), (2), (3) and (4) (referred to as I_s, I_L, I_H and I_{so} , respectively) in the brace denote the short-, long-wave radiation terms, the sensible heat and soil heat fluxes. The equation is solved with an iteration scheme, and the solution is converged easily. I_∞ is the solar constant, h the depth of the temperature wave in the soil and $h = 10$ cm is used. In estimation of term I_s , an experimental parameter $\mu = 0.75(1-A)$ is used, and A is the solar albedo (Schlunzen, 1990). $\hat{\varepsilon}$ is the reducing factor of long-wave radiation and $\hat{\varepsilon} = 0.32$ is used, which is determined according to the diurnal temperature range of Qingdao in the early winter. k_s and γ_s are the thermal diffusivity and conductivity of soil. The remaining symbols have their normal meanings in meteorological parlance. The influence of the sloping terrain on the amount of shortwave radiation that reaches the ground is taken into account in the surface heat budget due to the calculation of the zenith angle $Z(t)$ (refer to Chapter 11, Pielke, 1984).

In order to estimate the boundary values of TKE and ε at the lower boundary, Mailhot (1982) and Duynderke (1988) schemes are employed with some modification due to the different positions of the bottom boundary:

$$\begin{aligned}
 E|_{z=z_0} &= 3.75u_*^2, & \eta_1 / L \geq 0 \\
 E|_{z=z_0} &= 3.75u_*^2 + 2.5(-\eta_1 / L)^{2/3} u_*^2, & \eta_1 / L < 0 \\
 \varepsilon|_{z=z_0} &= u_*^3 / L_{e0}(1 + 5\eta_1 / L), & \eta_1 / L > 0 \\
 \varepsilon|_{z=z_0} &= u_*^3 / L_{e0}, & \eta_1 / L \leq 0
 \end{aligned}$$

where L is Monin–Obukhov length, $\eta_1 = 10$ m. L_{e0} is the dissipation length at the lower boundary and set $L_{e0} = 0.10$ m.

It is known from the measured wind rose that the prevailing wind directions in Qingdao are in the south and north, and that the wind direction varies with seasons. The prevailing wind directions are S and SSE in spring and summer, N and NW in winter. However, a main direction of wind in autumn is not prominent, but the wind frequency in the N, NW, SW, S and ENE sectors is greater compared to the other sectors (after Long, personal communication).

In the following sections, the simulated results for Qingdao's local winds are discussed for different background synoptic conditions. It is assumed in the model calculation that $\partial U_g / \partial z = \partial V_g / \partial z = 0$. The synoptic scale meteorological fields and the sea surface temperature (SST) are kept steady in each test. The synoptic potential temperature field is assumed to be stably stratified ($\gamma = 0.0035$ K/m), corresponding to the mean situation in middle latitudes.

The main aim of this group of tests is to study the structural features of up- and down-slope winds of Laoshan mountains and sea-land-breezes of Jiaozhou Bay and the interaction of both in December, corresponding to a solar declination of $\delta = -23.0^\circ$. In these experiments the simulations are performed in W–E vertical cross-section. The x direction is in the east, y points to the north. The width of Jiaozhou Bay is taken as 21.25 km, and the eastern shoreline is located at $x=0$, as pointed out by an arrow in Fig.2. $U_g=0$, $V_g=3.0$ m/s for test 1; $U_g=0$ and $V_g=-3.0$ m/s for test 2; $U_g=1.5$ m/s, $V_g=0$ for test 3. The sea surface temperature is set equal to the surface value of the synoptic scale temperature profile and $SST = 278.5$ K, which is nearly equal to its normal value in the early winter.

For accomplishing initialization over the irregular terrain, a two-step procedure is employed. Firstly, the synoptic background wind and temperature profiles are adjusted to match to each other by used of a one-dimensional version of the model; Secondly, the adjusted temperature values are distributed there in a horizontally homogeneous way, and the so-called "diastrophism" procedure (Pielke, 1984) is used to permit the terrain growing to its assigned height in 6 hours, and a similar procedure to the "diastrophism" is applied to background wind profile to permit it to grow to the adjusted values during the first 3 hours, in order to match temperature and wind fields to the terrain.

The initial value of turbulent kinetic energy is diagnostically calculated, based on the assumption of balance between the production and dissipation of TKE at $t=0$ and with the aid of mixing length idea (Wu, 1987):

$$\begin{aligned}
 K_m &= l(0.2E)^{1/2}, \\
 E &= 5ll_e S^2 v(1 - \alpha_H Ri),
 \end{aligned}$$

$$\varepsilon = (c_2 E)^{3/2} / l_r,$$

where the mixing-length l is set 20 m above the 100 m level and decreases linearly below that level; $c_2 = 0.2$, l_r is the dissipation length, and $l_\varepsilon = 0.44l$ with the aid of Eq. (7). $\alpha_H = 1.35$ is used, Ri is the gradient Richardson number, and

$$S^2 v = \left(\frac{\partial \bar{u}}{\partial z} \right)^2 + \left(\frac{\partial \bar{v}}{\partial z} \right)^2.$$

At $t = 0$, no mesoscale perturbations of wind components, temperature, pressure and density are present in the whole integration domain.

3. Grid Structure and Integration Scheme

The equations are solved on an ARAKAWA-C staggered grid (Schlunzen, 1988), and a fine-mesh uniform horizontal grid of $\Delta x = 1.25$ km is utilized within an area of 50 km centered at $x = 0$. Beyond this area, Δx is increasing gradually $\Delta x_{j+1}(\Delta x_{j-1}) \approx 1.25 \Delta x_j$ up to 5.0 km at the lateral boundary areas. In the vertical direction 29 levels are utilized. The grid increment $\Delta \eta$ is slowly enlarged with height from 20 m close to the surface, up to 500 m close to the model top at $z_{\text{top}} = 8.4$ km.

Since we are not interested in the phenomena occurring in the east side of the ridge of Laoshan mountains and for avoiding the calculation troubles caused by sharp slope, the terrain in the east of the mountain ridge is artificially smoothed. A flat terrain replaces the sharp slope and the sea area.

The solution of the equations in the main model is described by Schlunzen (1990) in detail. For the numerical integration of the TKE- and ε -equations a splitting-up scheme is used. The advection terms are solved in the way as in the main model following Smolarkiewicz and Clark (1986). The vertical diffusion and dynamic adjustment terms in the E- ε equations are solved with a reweighted Crank-Nicolson scheme.

III. ANALYSES OF THE SIMULATED RESULTS

For comparison of the model results with measurements, it is necessary to look at some observed results. It is found from the observations that the prevailing wind at station A (see Fig. 1) is easterly at night and early morning, owing to effects of the down-slope wind of Laoshan mountains and some small hills. The basic features of the flow observed at station A are shown in Table 1.

It is found from Table 1 that generally the down-slope wind starts after 2000 LST and collapses after the sunrise. February, June and July, as well as October to December are less down-slope wind periods. Partly this can be explained by a higher frequency of foggy and rainy days in June and July. In winter (October to February), however, the frequency of down-slope winds might be reduced due to the influence of active cold air and the prevailing northerly wind. This will be discussed in detail later. Notice that, when figures are discussed in the following, the solid lines represent the positive values, and the dashed lines the negative values.

Fig. 2 shows the mesoscale temperature field at 1400 LST of test 1, which corresponds to the fully developed stages of the sea breeze and the up-slope winds. Fig.3 shows the vertically

Table 1. The Monthly Mean Features of the Down-Slope Wind (ENE-ESE) Observed at the Synoptic Station A (November 1985—October 1987)

Month	Frequency (d / mon)	Speed (m / s)	Collapsed time (LST)*	Duration (h)
1	10.0	3.0	0630	8.7
2	7.0	2.9	0745	11.2
3	10.5	3.5	0720	8.9
4	11.0	3.3	0710	9.0
5	12.0	3.3	0650	10.2
6	8.0	2.8	0645	9.2
7	7.0	3.2	0610	8.6
8	12.0	2.5	0705	9.4
9	9.5	3.2	0655	8.0
10	7.0	3.2	0715	8.8
11	7.5	2.8	0750	10.5
12	4.5	3.5	0800	10.3

* LST is local standard time.

turbulent exchange coefficient field of test 1 for the corresponding time to Fig. 2.

In comparison, it is found that the calculated mesoscale potential temperature fields of test 2 (figures omitted) result in similar structural features to test 1. The difference in exchange coefficient fields for both tests is that test 1 shows a slightly stronger maximum than test 2 at 0800 LST, however, an inverse situation is present at 1400 LST. The maxima of the turbulent exchange coefficient K_m are situated in the areas controlled by the major mesoscale circulations, as shown in Fig. 3.

Additionally, the simulated results show that the used model can reasonably describe the surface temperature variations over a complex terrain, e.g. the temperature is lower in a valley than at its both slopes at night; the temperature at the eastern slope is higher than at the western slope from the sunrise to about 1500 LST, as shown in Fig.2; and the calculated mesoscale

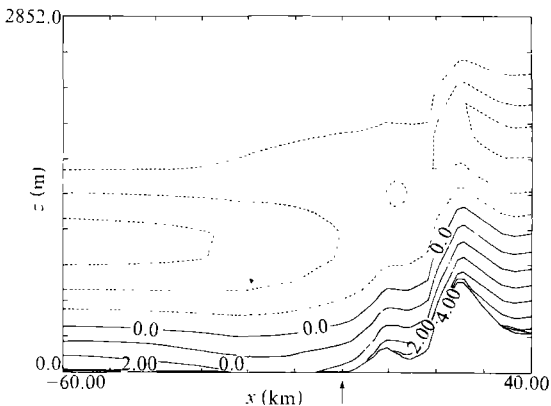


Fig. 2. The mesoscale temperature fields (K) of test 1 at 1400 LST corresponding to the strongest period of the up-slope wind and sea breeze; contour interval 0.5 K.

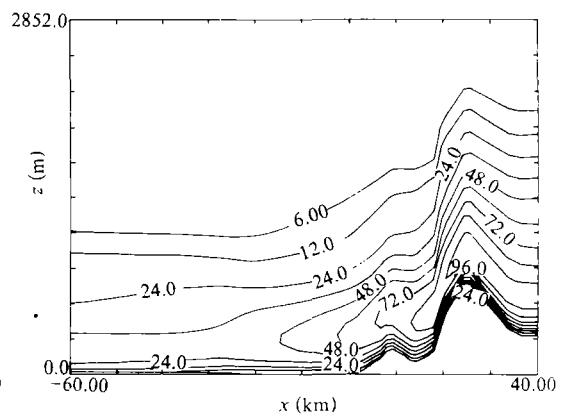


Fig. 3. As in Fig. 2, but for the vertical turbulent exchange coefficient fields (m^2/s) at 1400 LST; contour interval $12.0 \text{ m}^2/\text{s}$.

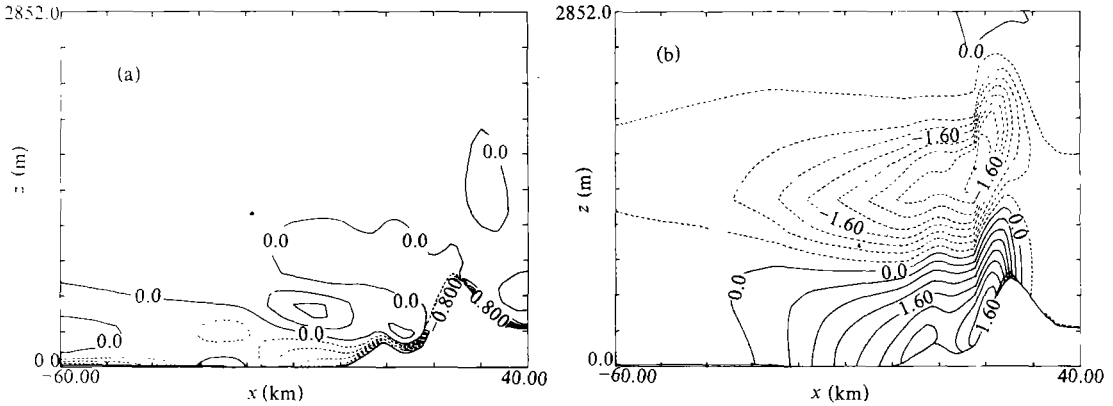


Fig. 4. The mesoscale wind component \tilde{u} (m/s) of test 1: (a) for 0800 LST; contour interval 0.2 m/s; (b) for 1400 LST; contour interval 0.4 m/s.

temperature structures around the coastlines are also convincing.

Fig. 4 presents the mesoscale wind component \tilde{u} fields at 0800 LST and 1400 LST, resulting from test 1. It is not difficult to understand the facts that the easterly wind of test 1 is stronger than test 2 shown in Fig. 5, and the westerly wind component in both tests shows a contrary feature to the above, since the contrary direction of the background winds results in different wind directions in the Coriolis force term (Wu, 1989).

Some observational results reveal that both down- and up-slope winds are most frequent with geostrophic winds of less than 6 m/s. Geostrophic wind greater than 6 m/s tends to swamp the mesoscale circulation, regardless of the direction of the background winds (Atkinson, 1981). The results are supported by the observations taken at station A. Based on the above conclusion and the calculated results shown in Fig. 4a, we can say that for a southerly geostrophic wind less than 6 m/s, the down-slope wind of Laoshan mountains can overpass station A and excite the land breeze circulation corresponding to the east shore of Jiaozhou Bay. This intensifies the land breeze at the east shore, and so the breeze is much stronger than that at the west shore.

It can be noticed in Figs. 4b and 5 that the sea breeze branch at the east coast of the Bay is much stronger than that at the west coast owing to the coupling of the sea breeze circulation at the east coast with the up-slope wind circulation at the west slope of Laoshan mountains.

The results of test 1 show that a southerly wind of 3.4 m/s develops at the 600 m level centered between Laoshan mountains and Jiaozhou Bay at 0800 LST. The southerly wind is getting stronger with time and moves up- and west-ward (figures not shown). At 1400 LST, \bar{v} reaches 4.2 m/s, as shown in Fig. 6a. The maximum is located at a height of 1400 m over Jiaozhou Bay. At 2000 LST, the center is over the west shore of the Bay at the 1700 m level and \bar{v} reaches 6.8 m/s.

Corresponding to the northerly geostrophic wind 3 m/s, the results of test 2 show that a mesoscale northerly wind is formed with the maximum at a height of about 250 m above the east coastline of the Bay (Fig. 6b), and a southerly wind center is located at about 1400 m level. However, it is interesting that the position of the southerly wind center is approximately unchanged in the whole day.

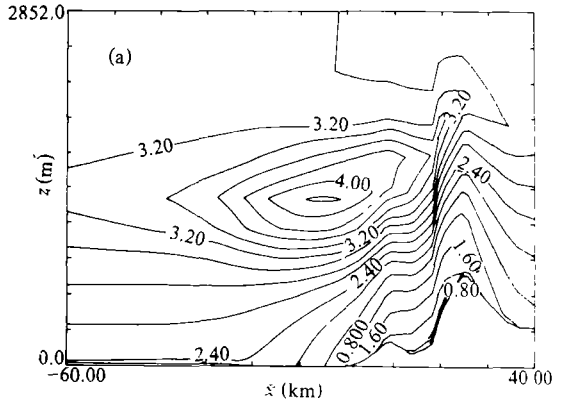
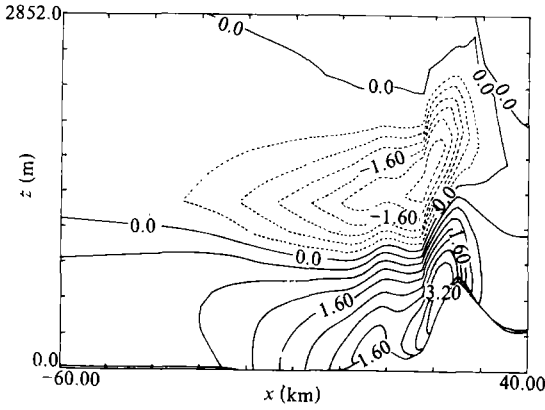


Fig. 5. The mesoscale wind component \bar{u} (m / s) of test 2, at 1400 LST; contour interval 0.4 m / s.

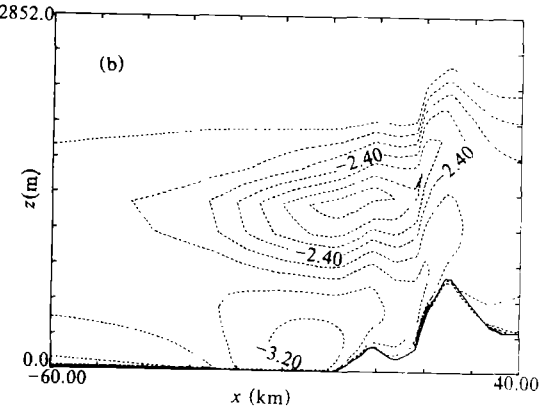


Fig. 6. The composite wind component \bar{v} (m / s) of meso- and synoptic scale winds at 1400 LST: (a) for test 1; contour interval 0.2 m / s; (b) for test 2; contour interval 0.2 m / s.

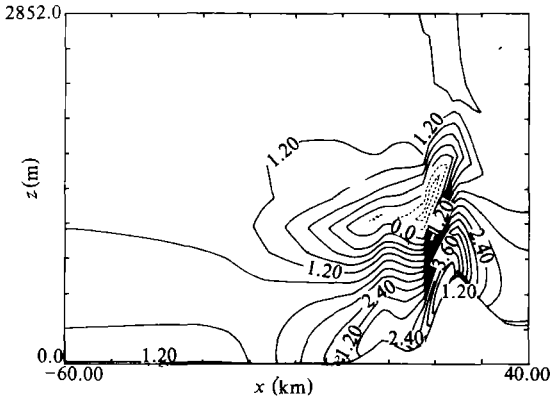


Fig. 7. The composite wind component \bar{u} (m / s) of the meso- and large-scale winds in test 3, at 1400 LST corresponding to the full developed stage of the sea breeze and up-slope wind; contour interval 0.3 m / s.

Fig.7 shows the calculated results of test 3, corresponding to a 1.5 m/s westerly geostrophic wind. Comparing the results at 0800 LST of test 3 with tests 1 and 2, it is found that in the early morning the down-slope wind of Laoshan mountains and the land breeze circulations corresponding to both coastlines of the Bay resulting from test 3 present similar features to test 2, but different from test 1. For the daytime the size and intensity of the mesoscale circulation corresponding to the east coast of the Bay, exhibited by Fig. 7 are much smaller and weaker than the other cases. We think, the difference can be attributed to the cold air advection caused by the westerly background wind, which reduces the atmospheric baroclinicity between the water surface and the land.

IV. CONCLUDING REMARKS

Based on the above analyses and discussions, we can reach the following conclusions:

(1) This model can reasonably simulate the surface temperature over a complex terrain as well as mesoscale circulations induced by topographic, thermodynamic, and mechanical effects, such as sea land breezes, slope and valley winds, and their interactions.

(2) When the geostrophic winds is a gentle southerly one, the down-slope wind of Laoshan mountains' western slope can usually arrive at the eastern coast of Jiaozhou Bay, and excite and intensify the land breeze in the early morning. However, when the geostrophic wind is in the opposite direction, the down-slope wind of the Laoshan mountains western slope gets much weaker than the former and is arrested at the foot of Laoshan mountains. This is the main reason for weakening the down-slope wind at the western slope of Laoshan mountains in the winter half year.

(3) After sunrise the sea breeze circulation generated at the eastern coast of Jiaozhou Bay is coupled with the up-slope wind at the western slope of Laoshan mountains and the coupled circulation is much stronger in the case with a gentle northerly geostrophic wind than with a southerly geostrophic wind.

(4) A gentle westerly background wind can reduce the sea breeze and up-slope wind circulations corresponding to the east coast of Jiaozhou Bay and to the west slope of Laoshan mountains, but it shows only a small effect on the land breeze and down-slope wind in the same area as the above.

Although the obtained results are convincing, some observed facts and phenomena show that a further observational and theoretical study on Qingdao's local winds is very necessary. It is particularly worth studying and examining the 3-dimensional structural features of the local wind, since the interaction between the sea breezes coming from the Huanghai Sea and from Jiaozhou Bay, the effects of the city heat island and the varying roughness, as well as the slope-valley wind make Qingdao's local wind structure very complicated, and these local structures obviously influence the transport of pollutants.

The authors would like to thank Prof. Dr. M. Schatzmann who showed a great interest and support to the study, thanks also to Dr. K. Bigalke and Prof. Long Baosen for effective comments. A special thank is devoted to Miss Zang Xiaohong for typing the manuscript.

REFERENCES

- Atkinson, B. W. (1981). *Mesoscale Atmospheric Circulations*, Academic Press London.
- Bodin, S. (1979). A predictive numerical model of the atmospheric boundary layer based on the turbulent energy equation, SMHI Rep. No. 13.
- Detering, H. W. and Etling, D. (1985). Application of the $E-\epsilon$ turbulence model to the atmospheric boundary layer, *Boundary Layer Meteor.*, **33**: 113—133.
- Dunst, M. (1980). Ergebnisse von Modellrechnungen zur Ausbreitung von Stoffbeimengungen in der planetarischen Grenzschicht, *Zeitschrift f. Meteorologie*, **30**: 47—59.
- Duynkerke, P. G. (1988). Application of the $E-\epsilon$ turbulence model to the neutral and stable atmospheric boundary layer, *J. Atmos. Sci.*, **45**: 865—879.
- Holt, T. and Ramam, S. (1988). A review and comparative evaluation of multilevel boundary parameterizations for

- first-order and turbulent kinetic energy closure schemes, *Reviews of Geophysics*, **26**: 761—780.
- Mailhot, J. and Benoit, R. (1982), A finite-element model of the atmospheric boundary layer suitable for use with numerical weather prediction. *J. Atmos. Sci.*, **39**: 2249—2266.
- Orlanski, I. (1976), A simple boundary condition for unbounded hyperbolic flows, *J. Comput. Phys.*, **21**: 251—269.
- Pepper, D. W., Keen, C.D. and Long, P. E. (1979), Modeling the dispersion of atmospheric pollution using cubic splines and Chapeau function, *Atmos. Env.*, **13**: 223—237.
- Pielke, R. A. (1984), *Mesoscale Meteorological Modeling*, Academic Press, New York.
- Schlunzen, K. H. (1988), *Das Mesoskalige Transport- und Stromungsmodell METRAS-Grundlagen. Validierung. Anwendung*, Hamb. Geophys. Einzelschriften, A88, University of Hamburg, F.R.G.
- Schlunzen, K.H. (1990), Numerical studies on the inland penetration of sea breeze fronts at a coastline with tidally flooded mudflats. *Beitrage Zur Physik der Atmosphere*, **63**: 243—256.
- Smolarkiewicz, P. K. and Clark, T. L. (1986), The multidimensional positive definite advection transport algorithm: Further development and applications, *J. Comp. Phys.*, **67**: 396—438.
- Wu Zengmao (1987), Numerical study of lake-land breeze over Lake Vattern Sweden. *Advances in Atmos. Sci.*, **4**: 198—209.
- Wu Zengmao (1989), Numerical analysis of the sea (lake) breeze dynamics and initialization of the model. *Acta Oceanologica Sinica*, **8**: 535—548.